Received: 12 August 2018 | Revised: 19 November 2018 | Accepted: 10 January 2019

DOI: 10.1002/dac.3924

RESEARCH ARTICLE

WILEY

Investigation of maximum lifetime and minimum delay trade-off in underwater sensor networks

Huseyin Ugur Yildiz

Department of Electrical and Electronics Engineering, TED University, Ankara, Turkey

Correspondence
Huseyin Ugur Yildiz, Department of Electrical and Electronics Engineering, TED University, 06420 Ankara, Turkey.
Email: hugur.yildiz@tedu.edu.tr

Summary

Underwater acoustic sensor networks (UASNs) are subjected to harsh characteristics of underwater acoustic channel such as severe path losses, noise, and high propagation delays. Among these constraints, propagation delay (more generally, end-to-end delay) is the most dominating limitation especially for time-critical UASN applications. Although the minimization of end-to-end delay can be achieved by using the minimum hop routing, this solution cannot lead prolonged lifetimes since nodes consume excessive energy for transmission over long links. On the other hand, the maximization of network lifetime is possible by using energy efficient paths, which consist of relatively short links but high number of hops. However, this solution results in long end-to-end delays. Hence, there is a trade-off between maximizing the network lifetime and minimizing the end-to-end delay in UASNs. In this work, we develop a novel multi-objective–optimization (MOO) model that jointly maximizes the network lifetime while minimizing the end-to-end delay. We systematically analyze the effects of limiting the end-to-end delay on UASN lifetime. Our results reveal that the minimum end-to-end delay routing solution results in at most 72.93% reduction in maximum network lifetimes obtained without any restrictions on the end-to-end delay. Nevertheless, relaxing the minimum end-to-end delay constraint at least by 30.91% yields negligible reductions in maximum network lifetimes.

KEYWORDS

end-to-end delay, integer linear programming, multi-objective optimization, network lifetime, underwater acoustic sensor networks

1 | INTRODUCTION

Typical underwater acoustic sensor networks (UASNs) applications can be categorized as time-critical applications (eg, coastline protection, submarine detection, military-assisted navigation, tactical surveillance, leakage detection, and mine reconnaissance[1-3]) and time-uncritical applications (eg, underwater-habitat monitoring and ocean-temperature tracking[1,2]). Regardless of the application category, UASNs are negatively affected by harsh impairments of the underwater environment such as long propagation delay, low bandwidth, high path loss, and frequent packet drops.[4] Among these impairments, the propagation delay is the most dominating constraint for time-critical UASN applications.

 © 2019 John Wiley & Sons, Ltd.

UASNs use acoustic (sound) waves for communications where the speed of sound is roughly 1500 m/s in underwater that is extremely slow as compared with electromagnetic waves.[5] The low propagation speed of sound results in high propagation delays, which drastically increase the end-to-end delay (ie, time required for data packets to travel from source nodes to the sink node). Moreover, high expenditure costs of underwater sensor nodes cause UASNs to be sparsely deployed.[6] Considering that the sparse deployment of sensor nodes results in long link distances, nodes consume excessive amount of energy for communications, which degrades both the network lifetime and the energy efficiency. Replacing or recharging the limited battery supplies of sensor nodes is infeasible since nodes can be deployed in remote or hard-to-reach areas of underwater.[7] In order to attain energy efficiency for a long-term operational network, sensor nodes need to deplete their battery energies in a balanced manner.[8]

One way of attaining the energy efficiency and extending the network lifetime is to use multi-hop communication techniques (ie, data packets are forwarded to the sink node by using intermediate relay nodes), which have positive impacts on reducing the communication energy consumption in a sparse UASN due to the decrement of link distances.[9] However, multi-hop communication leads in high end-to-end delay because of the increment of the hop count.[10] On the other hand, the minimum end-to-end delay routing strategy imposes the usage of suboptimal paths, which contain low number of hops. Nonetheless, this solution dramatically increases the communication related energy dissipation hence negatively effects the network lifetime due to the extreme transmission energy cost of underwater sensor nodes for communicating over longer links.[11] Hence, the minimization of end-to-end delay and the maximization of network lifetime creates a trade-off in UASNs such that maximum network lifetimes cannot be achieved by using the minimum end-to-end delay routing.

In this work, we systematically explore the minimization of end-to-end delay and maximization of network lifetime trade-off in UASNs, which has never been addressed in UASN literature before. More precisely, our novel contributions are enumerated as follows:

1. We propose a multi-objective–optimization (MOO) model, which maximizes the network lifetime while minimizing the end-to-end of the network. The developed MOO model is built by using integer linear-programming (ILP) formulations. The MOO model employs the foundations of underwater communication channel principles by using the power consumption characteristics of the Woods Hole Oceanographic Institution (WHOI) Micromodem,[12] which is a widely used underwater modem for both industrial and research applications. Moreover, a detailed link-layer energy-consumption model is incorporated into the MOO model.
2. By solving the proposed MOO model, we explore the deterioration of maximum network lifetime (ie, lifetime obtained without any constraints on the end-to-end delay) caused by the minimum end-to-end delay routing.
3. We investigate the amount of decrement in the maximum network lifetime by gradually relaxing the minimum end-to-end delay constraint. We also determine the amount of relaxation in the minimum end-to-end delay to achieve the maximum network lifetime.

The structure of this paper is provided as follows. Section 2 overviews the literature on the usage of optimization methods for time-critical UASNs. Our system model, which includes the link-layer energy consumption model as well as the MOO framework, is detailed in Section 3. In Section 4, solutions of the MOO model are discussed. Finally, Section 5 provides the conclusions of this work.

2 | RELATED WORK

A considerable amount of literature has been published on the usage of optimization methods for time-critical UASNs in recent years. In these works, the objective functions of the proposed optimization models are generally defined as (a) the minimization of end-to-end delay (eg, previous studies[4,5,13-18]), (b) the minimization of energy consumption (eg, previous studies[2,5,7,15,18-20]), and (c) the maximization of network lifetime (eg, previous studies[4,21-23]). Some constraints of these optimization models include the per-node flow-balance constraint (ie, flows are balanced at each node), the end-to-end flow conservation constraint (ie, every generated data are terminated at the sink node), the energy capacity constraint (ie, amount of energy consumed by nodes are limited), data-capacity constraint (ie, the capacity of each link is bounded), and the delay constraint (ie, end-to-end delay of the network is limited), which are either defined as separate constraints[2,7,9,20,22-24] or incorporated into some constraints (eg, per-flow balance).[25-27]

Some applications of optimization methods used in time-critical UASNs include routing protocol development[2,10,14,24,25] and optimal relay-node deployment. The surface-level gateway node-deployment problem[4,5,13,15,18,21,28] can be considered

as an example of optimal relay-node deployment. In this approach, ordinary sensor nodes convey their data to the nearest surface-level gateway. Surface-level gateways then use electromagnetic waves to transfer data to the central base station within negligible times and low energy costs. This problem is modeled by using ILP where the aim is to determine the minimum number and optimal locations of surface gateways such that the delay[4,5,13,15,18,28] or the energy consumption is minimized.[5,15,18,28] The objective can be also be the maximization of network lifetime as in previous research.[4,21] Similar to the surface-level gateway deployment problem, there are also several studies in the literature that aim to achieve an optimal deployment strategy of relay nodes,[16] mobile-sink based data collectors,[6,19,22,27] and autonomous underwater vehicles[17,23] for time-critical UASNs.

Recently, a considerable literature has grown up around the reliability of communications for time-critical UASNs, which is investigated within packet delivery ratio (PDR)[7,25] and retransmission[9,15,20,22,25,29] perspectives. In other studies,[7,25] authors enforce a constraint for a PDR threshold to be satisfied in their optimization models. In previous works,[9,29] authors consider an infinite retransmission mechanism and jointly optimize the signal-to-noise ratio (SNR), frequency, and code rate for minimizing the energy cost of a transmitted bit with delay constraints. In another research,[30] the same topic is investigated where retransmissions are not allowed.

Many time-critical UASNs related research use a well-known empirical formulation to model underwater propagation losses.[2,4,5,7,17-20,22,25,26] However, there is a large volume of published works that ignore to model propagation mechanisms of underwater environment at the physical layer (eg, previous research[13-16,21,23,24,27,28]). Moreover, frequent packet drops are considered in some works[2,7,16,17,19,20,22,25] but assumed to be neglected in many of the works (eg, other studies[4,5,13-15,18,21,23,24,26-28]). There are only a few works that incorporate either retransmission or PDR thresholds for a reliable communication performance[15,17,20,22,25] in delay constrained UASNs. A significant number of works either assumes a fixed transmission power or uses simplifying assumptions to determine the energy costs without adopting the energy dissipation characteristics of a real underwater node platform at the link-layer (eg, other works[5,13-16,18,21,24,28]). From a different perspective, a low-cost hardware approach called SecureTag is proposed in the previous study.[31] SecureTag is used to improve the protection of on-body Internet-of-Things devices by using the propagation features of distinct creeping waves. On the other hand, upper-layer impact of nonorthogonal multiple access on the user side is systematically investigated in an existing literature.[32]

Unlike the existing works, which are focusing on routing protocol development, optimal relay-node deployment, and etc, by using optimization methods in time-critical UASNs, our work differs from previous studies in several aspects. First, the aim of this paper is to explore the minimum end-to-end delay and the maximum UASN lifetime trade-off. For this purpose, we jointly model severe underwater physical-layer channel conditions and link-layer energy costs by using a real underwater node platform while satisfying a certain communication performance via retransmissions. Second, we built a novel MOO framework for joint optimization of the network lifetime as well as the end-to-end delay by employing the aforementioned physical and link-layer models. Third, we quantitatively analyze the effects of limiting the end-to-end delay on the UASN lifetime by using the proposed MOO framework. To the best of our knowledge, the trade-off between the minimum end-to-end delay and the maximum network lifetime in UASNs has never been investigated in such a systematic way in the literature before.

3 | SYSTEM MODEL

In this section, we present our energy-consumption model and the MOO model, which is built by using ILP formulations. Throughout this work, we use the energy-consumption characteristics of WHOI Micromodem,[12] which is a commonly used underwater modem for both industrial and research applications.

3.1 | Energy-consumption model

3.1.1 | Underwater-propagation model

We use the passive sonar equation to model underwater sound propagation.[7] In this model, the SNR at the receiving node j (where the transmitter is denoted as node-i) can be calculated as

$$\overline{\mathrm{SNR}_{ij}(m,f)} = \overline{\mathrm{SL}(m,f)} - \overline{N(f)} - \overline{A_{ij}(f)} \geq \overline{\mathrm{SNR}_{tgt}}, \tag{1}$$

where $\overline{\mathrm{SL}(m,f)}$ is the sound source level of the transmitter node-i (in dB re 1μPa) using the power level m, $\overline{N(f)}$ is the power spectral density of the ambient noise (in dB), and $\overline{A_{ij}(f)}$ is the transmission loss in link (i,j) (in dB). Note that,

$f = 25$ kHz is the central operating frequency of WHOI Micromodems.[12] $\overline{\text{SNR}_{tgt}} = 10$ dB is the targeted SNR at the receiver node j.[10] The sound source level can be calculated as

$$\overline{\text{SL}(m,f)} = 10\ \log_{10}\left(\frac{P_{tx}(m)}{2\pi H I_0}\right), \tag{2}$$

where $I_0 = 0.67 \times 10^{-18}$ is the reference intensity,[3] H is the depth of the water, and $P_{tx}(m)$ is the electrical transmission power at discrete power level m (in Watts). We define $\mathcal{M}$ to denote the discrete power level set of WHOI Micromodems. Note that, WHOI Micromodems have transmission powers between 8 and 48 W.[12] We assume that there are 11 discrete power levels available (ie, $\mathcal{M} = \{8\ \text{W}, 12\ \text{W}, \ldots, 48\ \text{W}\}$).

The transmission loss in link-(i,j) is expressed as

$$\overline{A_{ij}(f)} = \overline{A_0} + 10\kappa\ \log_{10}(d_{ij}) + d_{ij} \times 10^{-3} \times \overline{\alpha(f)}, \tag{3}$$

where $\overline{A_0} = 30$ dB is the transmission anomaly,[33] $\kappa = 1.5$ is the spreading factor,[34] d_{ij} is the distance of the link (i,j) in meters, and $\overline{\alpha(f)}$ is the absorption coefficient (in dB/km), which is calculated by using Thorp's equation[35] as

$$\overline{\alpha(f)} = \frac{0.11 f^2}{1+f^2} + \frac{44 f^2}{4100+f^2} + 2.75 \cdot 10^{-4} f^2 + 0.003. \tag{4}$$

The noise-power spectral density is composed of four sources: turbulence, shipping, waves, and thermal noise. For simplicity, the noise-power spectral density can be approximated as

$$\overline{N(f)} \approx 50 - 18\ \log_{10}(f). \tag{5}$$

WHOI Micromodems employ binary phase-shift keying (BPSK) where the bit error rate for this modulation scheme when considering a Rayleigh fading channel is defined as[7]

$$p^b_{ij}(m,f) = \frac{1}{2} - \frac{1}{2}\sqrt{\frac{\text{SNR}_{ij}(m,f)}{1+\text{SNR}_{ij}(m,f)}}. \tag{6}$$

In this equation, $\text{SNR}_{ij}(m,f)$ is given in ordinary form. For a data packet length of L_P bits, the success probability of packet transmission by using the power level-l_D (where $l_D \in \mathcal{M}$) is calculated as

$$p^s_{D,ij}(l_D,f) = (1 - p^b_{ij}(l_D,f))^{L_P}. \tag{7}$$

Similarly, for an L_A bits of acknowledgement (ACK) packet, the corresponding success probability of ACK transmission by using the power level l_A (where $l_A \in \mathcal{M}$) is $p^s_{A,ij}(l_A,f) = (1 - p^b_{ij}(l_A,f))^{L_A}$. We define $p^f_{D,ij}(l_D,f)$ and $p^f_{A,ij}(l_A,f)$ to represent fail probabilities of data and ACK transmissions, respectively. From hereafter, we omit the f notation in the rest of the paper since f is taken as constant. Considering a two-way handshake process (ie, data packets are replied with ACK packets), the success handshake probability can be expressed as

$$p^s_{HND,ij}(l_D,l_A) = p^s_{D,ij}(l_D) \times p^s_{A,ji}(l_A). \tag{8}$$

For a reliable communication performance to compensate packet losses, we employ a retransmission mechanism where the energy cost of transmission and reception are scaled by $\lambda_{ij}(l_D,l_A) = \frac{1}{p^s_{HND,ij}(l_D,l_A)}$ whenever a failed transmission is occurred.[9]

3.1.2 | Link-layer model

We assume a slotted link-layer model where the network operation time is divided into equal duration of rounds.[36] Each round lasts for $T_R = 70$ seconds.[2] The active time slot of a link (i,j) is calculated as $t^s_{ij} = \frac{L_P}{R} + t^p_{ij} + \frac{L_A}{R}$. In this calculation, $t^p_{ij} = 2 \times \frac{d_{ij}}{c}$ is the round-trip propagation delay accounted for both data and ACK-packet transmissions on link-(i,j) where $c = 1500$ m/s is the nominal speed of sound in water.[5] $\frac{L_P}{R}$ and $\frac{L_A}{R}$ are times required to transmit $L_P = 1024$ bits of a data

packet,[3] and $L_A = 88$ bits of an ACK packet[9] where $R = 5$ kbps is the data rate of WHOI Micromodems.[12] Note that, the delay component consists of both transmission and propagation delays, respectively.

The transmitter node i dissipates $P_{tx}(l_D)\frac{L_P}{R}$ of energy for transmitting L_P bits of a data packet by using the power level-l_D and $P_{rx}\frac{L_A}{R}$ of energy to receive an ACK packet from the receiver node j where $P_{rx} = 1$ W is the reception power of WHOI Micromodems.[30] In the rest of the slot time, node i spends $P_{std}(t^s_{ij} - \frac{L_P}{R} - \frac{L_A}{R})$ of energy to stay in the idle mode where $P_{std} =$ 80 mW is the power cost of WHOI Micromodems to stay in idle mode.[12] Hence, the total energy dissipation of node i in a successful handshake is calculated as

$$E^s_{tx,ij}(l_D) = P_{std}\left(t^s_{ij} - \frac{L_P}{R} - \frac{L_A}{R}\right) + P_{tx}(l_D)\frac{L_P}{R} + P_{rx}\frac{L_A}{R}. \tag{9}$$

If the handshake process has failed due to the data-packet errors on the forward link, $P_{tx}(l_D)\frac{L_P}{R}$ of energy still be consumed by node i; however, node i does not dissipate energy for ACK reception since an ACK packet would not be transmitted by node j (because node j cannot successfully receive a data packet). Similarly, if ACK packets have errors on the reverse link, then node i does not again dissipate energy for ACK reception. Thus, node i stays in the idle mode for $\left(t^s_{ij} - \frac{L_P}{R}\right)$ seconds while consuming $P_{std}\left(t^s_{ij} - \frac{L_P}{R}\right)$ of energy. Considering these two cases, corresponding retransmission ratios can be expressed as $\frac{p^f_{D,ij}(l_D)}{p^s_{HND,ij}(l_D,l_A)}$ and $\frac{p^s_{D,ij}(l_D)p^f_{A,ji}(l_A)}{p^s_{HND,ij}(l_D,l_A)}$, respectively. As a summary, if the handshaking has failed because of either data packet drops or ACK packet drops, the energy dissipation of node i can be expressed as

$$E^f_{tx,ij}(l_D,l_A) = \left[P_{std}\left(t^s_{ij} - \frac{L_P}{R}\right) + P_{tx}(l_D)\frac{L_P}{R}\right] \times \left(\frac{p^f_{D,ij}(l_D) + p^s_{D,ij}(l_D,l_A)p^f_{A,ji}(l_A)}{p^s_{HND,ij}(l_D,l_A)}\right). \tag{10}$$

Totally, node i spends

$$E^{tx}_{ij}(l_D,l_A) = E^s_{tx,ij}(l_D) + E^f_{tx,ij}(l_D,l_A), \tag{11}$$

of energy for transmission. Contrarily, the receiver node j dissipates $P_{rx}\frac{L_P}{R}$, $P_{tx}(l_A)\frac{L_A}{R}$, and $P_{std}\left(t^s_{ji} - \frac{L_P}{R} - \frac{L_A}{R}\right)$ of energies for the data-packet reception, the ACK-packet transmission, and staying in the idle mode if the handshake is successful, respectively. We denote

$$E^s_{rx,ji}(l_A) = P_{std}\left(t^s_{ji} - \frac{L_P}{R} - \frac{L_A}{R}\right) + P_{rx}\frac{L_P}{R} + P_{tx}(l_A)\frac{L_A}{R}, \tag{12}$$

to represent the total energy consumption for reception if the handshaking is successful. If the handshaking is unsuccessful due to the ACK-packet errors on the reverse link, the energy dissipation of node j can be calculated as

$$E^{f_1}_{rx,ji}(l_D,l_A) = \left[P_{std}\left(t^s_{ji} - \frac{L_P}{R} - \frac{L_A}{R}\right) + P_{tx}(l_A)\frac{L_A}{R} + P_{rx}\frac{L_P}{R}\right] \times \frac{p^s_{D,ij}(l_D)p^f_{A,ji}(l_A)}{p^s_{HND,ij}(l_D,l_A)}. \tag{13}$$

On the other hand, if the handshaking is unsuccessful due to the packet errors on the forward link, node j stays in the idle mode during the whole slot time since node j cannot receive the data packet (thus cannot send an ACK packet). In this case, node j consumes

$$E^{f_2}_{rx,ji}(l_D,l_A) = P_{std} \times t^s_{ji} \times \frac{p^f_{D,ij}(l_D)}{p^s_{HND,ij}(l_D,l_A)}, \tag{14}$$

of energy. As a summary, node j spends

$$E^{rx}_{ji}(l_D,l_A) = E^s_{rx,ji}(l_A) + E^{f_1}_{rx,ji}(l_D,l_A) + E^{f_2}_{rx,ji}(l_D,l_A), \tag{15}$$

of energy for reception.

3.2 | MOO model

In this part, we present our MOO model, which jointly maximizes the lifetime while minimizing the end-to-end delay of the network. UASNs considered in this work are composed of $|W|$ sensor nodes and a single base station (node 1).

We define W and V to represent the sets of sensor nodes and all nodes (including the base station), respectively. The set of links of the network is denoted by E. The amount of data packets flowing on link (i,j) that is generated at node l is denoted by an integer variable g_{ij}^{l}. We define the free variable, N_R to represent the network lifetime (ie, time until the first node exhausts its battery energy) in terms of rounds. Note that, the actual network lifetime can be calculated as $N_R \times T_R$ in terms of seconds. We define the variable, D to represent the average end-to-end delay (ie, time required for a data packet to travel from a source node to the sink node, which is averaged for all source sensor nodes). Hence, the objective functions of our MOO model are defined as

$$\text{Maximize} \quad N_R. \tag{16}$$

$$\text{Minimize} \quad D. \tag{17}$$

The constraints of our MOO framework are presented in (18) to (27).

$$\sum_{\substack{j\in V\\ i\neq j}} g_{ij}^{l} - \sum_{\substack{j\in W\\ i\neq j}} g_{ji}^{l} = \begin{cases} N_R \text{ if } & i = l \\ -N_R \text{ if } & i = 1 \\ 0 \text{ o.w.} & \end{cases}, \qquad \forall i \in V, \forall l \in W \tag{18}$$

$$\sum_{j\in W} g_{jl}^{l} = 0, \qquad \forall l \in W, \tag{19}$$

$$T_{act}^{i} = \sum_{l\in W}\left(\sum_{j\in V} g_{ij}^{l} t_{ij}^{s} \lambda_{ij}(l_{D,ij}^{opt}, l_{A,ji}^{opt}) + \sum_{j\in W} g_{ji}^{l} t_{ji}^{s} \lambda_{ji}(l_{D,ij}^{opt}, l_{A,ji}^{opt})\right), \qquad \forall i \in W, \tag{20}$$

$$\sum_{l\in W}\left(\sum_{j\in V} g_{ij}^{l} E_{ij}^{tx}(l_{D,ij}^{opt}, l_{A,ji}^{opt}) + \sum_{j\in W} g_{ji}^{l} E_{ji}^{rx}(l_{D,ij}^{opt}, l_{A,ji}^{opt})\right) + P_{hbr} \times \left(N_R \times T_R - T_{act}^{i}\right) \leq \xi, \quad \forall i \in W, \tag{21}$$

$$T_{act}^{i} \leq N_R \times T_R, \quad \forall i \in W, \tag{22}$$

$$\sum_{l\in W}\sum_{(i,j)\in E} g_{ij}^{l} \lambda_{ij}(l_{D,ij}^{opt}, l_{A,ji}^{opt}) t_{ij}^{s} = |W| \times \underbrace{Z}_{=D\times N_R}, \tag{23}$$

$$Z \geq N_R \times D^{L}, \tag{24}$$

$$Z \leq N_R \times D^{U}, \tag{25}$$

$$g_{ij}^{l} = 0 \quad \text{if} \quad d_{ij} > R_{max}, \qquad \forall (i,j) \in E, \forall l \in W, \tag{26}$$

$$g_{ij}^{l} \geq 0, \qquad \forall (i,j) \in E, \forall l \in W. \tag{27}$$

Constraint (18) is used to balance data flows at each source node (ie, if $i = l$), the base station (if $i = 1$), and relay nodes (ie, if $i \neq l$ and $i \neq 1$), respectively. We assume that a single data packet is generated at each round (with length L_P bits); hence, N_R packets are generated during the network lifetime. Constraint (19) prevents loops, which states that the generated data packet at node l cannot be terminated at node l. Constraint (20) is used to calculate the active time of a sensor node i (ie, T_{act}^{i}), which is defined as the summation of times required for both transmissions and receptions including the effects of retransmissions. We consider a power adjustment scheme in which we determine optimal discrete power levels for data and ACK packets that satisfy the targeted SNR value (ie, $\overline{\text{SNR}_{tgt}} = 10$ dB[10]) such that the total energy dissipation of transmission and reception on link (i,j) (ie, $E_{ji}^{tx}(l_D, l_A) + E_{ji}^{rx}(l_D, l_A)$)[36] is minimized. We denote $l_{D,ij}^{opt}$ and $l_{A,ji}^{opt}$ to represent the optimal transmission power levels used on link (i,j) for data and ACK-packet transmissions, respectively. Constraint (21) limits the amount of energy dissipated at each sensor node to the initial battery energy (ie, $\xi = 1$ MJ[5]). In this constraint, $E_{ij}^{tx}(l_{D,ij}^{opt}, l_{A,ji}^{opt})$ and $E_{ji}^{rx}(l_{D,ij}^{opt}, l_{A,ji}^{opt})$ values are obtained by plugging the optimal power levels $l_{D,ij}^{opt}$ and $l_{A,ji}^{opt}$ into Equations (11) and (15), respectively. Moreover, $P_{hbr} = 220\ \mu W$ is the power required for WHOI Micromodems to stay in hibernation mode.[12] Note that a sensor node stays in hibernation mode for a duration of $(N_R \times T_R - T_{act}^{i})$ seconds.

Constraint (22) ensures that the active time of a sensor node i cannot be greater than the network lifetime. Constraint (23) is used to calculate the average end-to-end delay of the network (ie, D). This equality can also be stated as

$$\frac{\sum_{l\in W}\sum_{(i,j)\in E} g_{ij}^{l}\lambda_{ij}(l_{D,ij}^{opt}, l_{A,ji}^{opt})t_{ij}^{s}}{|W|\times N_R} = D, \tag{28}$$

where the numerator of the left-hand side (LHS) of Equation (28) shows the elapsed time for all packets generated at all sensor nodes to reach the base station during the lifetime. Denominator of this expression calculates the average time required for a single packet generated in a single round to reach the base station. In constraint (23), we have a nonlinearity due to the product of two variables (ie, $D \times N_R$). In order to linearize the multiplication of two variables, we define a new continuous variable, Z, which is equal to $D \times N_R$. Assume that the average end-to-end delay has lower and upper bounds of D^L and D^U, respectively (ie, $D^L \leq D \leq D^U$). If we multiply both sides of $D^L \leq D \leq D^U$ by N_R, we obtain $N_R \times D^L \leq \underbrace{D \times N_R}_{=Z} \leq N_R \times D^U$. Hence, we include constraints (24) and (25) in our MOO framework to linearize the product of two variables. If this optimization problem is solved in terms of Z and N_R, D can be easily obtained by $D = \frac{Z}{N_R}$. Constraint (26) states that nodes cannot transmit farther than $R_{max} = 5$ km.[27] Finally, constraint (27) states that the amount of data flows cannot be negative.

In the proposed MOO framework, the objectives cannot be optimized simultaneously. A common way to determine solutions for MOO problems is to convert the original MOO problem into a MOO problem. In this work, we utilize the *ε-constraint method*.[37] In this method, one of the objective functions is optimized while other objectives are defined as constraints. We choose to maximize the network lifetime while the minimization of average end-to-end delay is defined as a constraint which is expressed as

$$\begin{aligned} &\text{Maximize} \quad N_R \\ &\text{subject to} \\ &\underbrace{D \leq \varepsilon}_{Z\leq \varepsilon N_R}, \\ &\text{Constraints in (18)– (27).} \end{aligned} \tag{29}$$

In this MOO problem, ε is the upper bound on the average end-to-end delay. In other words, ε is used to model the amount of relaxation of the minimum end-to-end delay constraint. Since D can be written as $\frac{Z}{N_R}$, $D \leq \varepsilon$ constraint can be redefined as $Z \leq \varepsilon N_R$. Although this constraint is similar to the constraint given in (25), the difference is that $\varepsilon \leq D^U$. In Section 4, we vary ε between D^L and D^U (*i.e.*, $\varepsilon \in [D^L, D^U]$) to investigate the impact of relaxing the minimum end-to-end delay constraint on network lifetime.

It is important to determine the ranges of the objective functions before solving the MOO problem to generate efficient solutions as ε varies. Let N_R^L and N_R^U be defined as lower and upper bounds of the objective N_R. Lower and upper bounds on D are already defined as D^L and D^U, respectively. We determine the lower and upper bounds of N_R and D as follows:

- When the optimization framework with the objective function (16) subject to the constraints (18) to (22), (26), and (27) is solved, we obtain N_R^U (ie, maximum network lifetime when there are no constraints on the end-to-end delay).
- If the optimization problem with the objective (17) subject to (18) to (23), (26), and (27) is solved when N_R is set as a parameter with $N_R = N_R^U$, the solution of this problem yields D^U (ie, upper bound on end-to-end delay when the network lifetime is maximum).
- In order to find D^L (ie, the minimum end-to-end delay of the network), we solve the same optimization problem (ie, optimization problem with the objective (17) subject to (18) to (23), (26), and (27)), where each sensor node generates a single packet per round (ie, N_R is treated as a parameter that is equal to 1).
- Finally, N_R^L (ie, network lifetime for the minimum end-to-end delay routing) can be obtained by solving the optimization problem with the objective function (16) subject to the constraints (18) to (23), (26), and (27) where D is treated as a parameter with the value $D = D^L$.

Note that, while determining the upper and lower bounds of N_R and D, N_R (or D) is treated as a parameter hence there is no need to use Z in the right-hand side of constraint (23) since $D \times N_R^U$ (or $D^L \times N_R$) becomes linear. As Z becomes needless, using constraints (24) and (25) is also unnecessary.

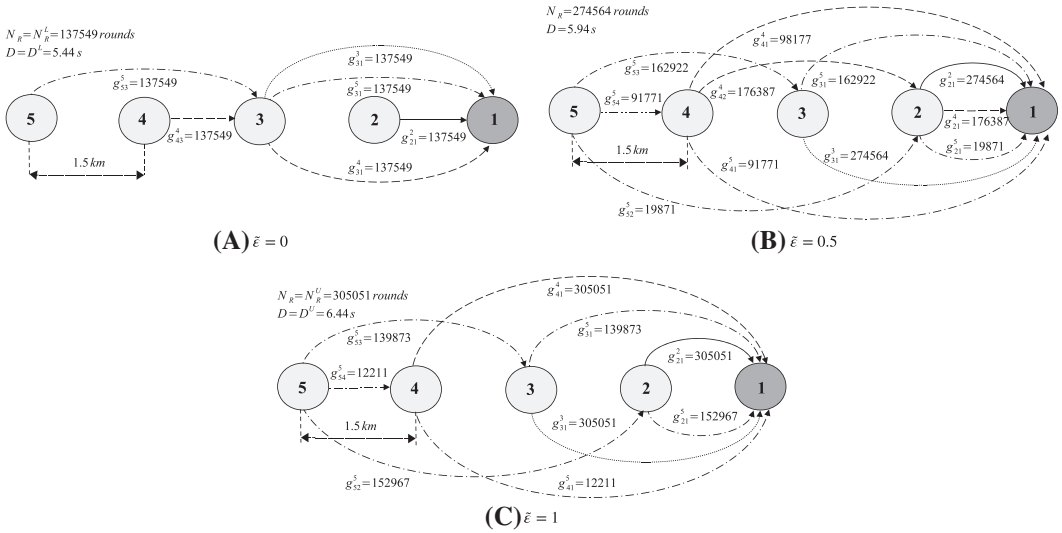

FIGURE 1 Solutions of the multi-objective–optimization (MOO) problem and on a five-node line network for the A, minimum end-to-end delay, B, the relaxed end-to-end delay routing, and C, the maximum network lifetime routing

4 | PERFORMANCE EVALUATION

In this section, we quantitatively investigate the trade-off between the maximum network lifetime and the minimum end-to-end delay for a large set of network configurations. The energy consumption model (Section 3.1) is developed in MATLAB*. The MOO problem (Section 3.2) is modeled and solved in GAMS by using the CPLEX 12 solver†.

4.1 | Toy example

We present the solutions of the MOO problem presented in (29) to determine optimal data flows that maximize the network lifetime while minimizing the end-to-end delay on a toy network in Figure 1. The toy network is constructed as a line network where five nodes are positioned such that internode distance is 1.5 km. Node 1 is chosen as the base station while nodes 2 to 5 are ordinary sensor nodes. We assume that all nodes have same depth (ie, $H = 50$ m). In each subfigure, solid, dotted, long-dashed, and dot-dashed line styles are used to represent optimum flows for nodes 2 to 5, respectively. We define $\tilde{\varepsilon}$ to model the amount of relaxation of minimum end-to-end delay which can be expressed as $\tilde{\varepsilon} = \frac{\varepsilon - D^L}{D^U - D^L}$. In this way, ε values are normalized between 0 and 1. For example, if $\varepsilon = D^L$ (ie, the minimum end-to-end delay routing), then $\tilde{\varepsilon} = 0$. On the other hand, if $\varepsilon = D^U$, then $\tilde{\varepsilon} = 1$ (ie, the maximum network lifetime obtained when there are no restrictions on the end-to-end delay). For the sake of simplicity, we choose $\tilde{\varepsilon} = 0$ in Figure 1A, $\tilde{\varepsilon} = 0.5$ in Figure 1B, and $\tilde{\varepsilon} = 1$ in Figure 1C, respectively.

In Figure 1A, we consider the minimum end-to-end–delay routing, hence we set $\tilde{\varepsilon} = 0$. In this case, the network lifetime is calculated as 137 549 rounds (ie, $N_R = N_R^L = 137\,549$ rounds) while the corresponding average end-to-end delay is observed as 5.44 seconds (ie, $D = D^L = 5.44$ seconds). Note that each sensor node generates a single data flow at each round, thus a total of 137 549 data flows (with size $L_P = 1024$ bits) are generated during the lifetime. Moreover, each node transmits its generated data to the base station by using a minimum number of hops. For example, node 5 uses 5-3-1 path to convey its generated data flows to the base station while node 3 directly transmits its data to the base station. In Figure 1B, we relax the minimum end-to-end delay constraint by setting $\tilde{\varepsilon} = 0.5$. In this case, the average end-to-end delay is increased to 5.94 seconds (increment of D^L by 9.19%) while the network lifetime is revealed as 274 564 rounds. Node 3 still uses the 5-3-1 path to convey its generated data to the base station. However, node 5 splits its generated data (274 564 flows) into three parts such that 162 922, 91 771, and 19 871 flows are conveyed to the base station by using paths 5-3-1, 5-4-1, and 5-2-1, respectively. Eventually, in Figure 1C, there are no constraints on the end-to-end delay (ie, $\tilde{\varepsilon} = 1$). In this network configuration, we obtain the maximum network lifetime as 305 051 rounds (ie, $N_R = N_R^U = 305\,051$ rounds) while the average end-to-end delay is 6.44 seconds (ie, $D = D^U = 6.44$ seconds). As a summary, this toy example

*https://www.mathworks.com/products/matlab.html
†https://www.gams.com/

shows that the minimum end-to-end delay routing strategy results in 54.91% lower network lifetimes than the maximum network lifetime obtained when there are no restrictions on the end-to-end delay. Moreover, our results also show that 18.38% increment in D^L yields N_R^U values.

4.2 | 3-D networks

In this part, we assume static 3-D UASNs,[1] which are composed of a single base station as well as $|W| = 20$, 30, and 40 sensor nodes that are uniformly distributed in a square area of $d_{net} \times d_{net}$ meters with a depth of H meters. Sensor nodes have random depths according to a uniform distribution, and nodes are assumed to be anchored to the bottom of the ocean. The base station is floating on the water surface, which is located in the middle of the square area. We take d_{net} in the interval of 2 to 10 km with an increment of 2 km. We consider five H values ranging from 50 to 1000 m to account for both shallow and deep water cases.[1] In order to investigate the impact of topological changes, each data point in Figures 2 to 6 is averaged over 100 randomly generated topologies.[13]

We present minimum end-to-end delays of the networks (D^L – in seconds) as a function of d_{net} with the five depth values (*i.e.*, $H = 50$, 200, 500, 750, and 1000 m) for $|W| = 20$ in Figure 2A, for $|W| = 30$ in Figure 2B, and for $|W| = 40$ in Figure 2C, respectively. Our analysis reveals that minimum end-to-end delays are in the interval 1.23 to 9.36 seconds regardless of the network topology. For a fixed $|W|$, D^L increases as d_{net} increases because to the increment of link distances, which results in both longer propagation delays and more hop counts to reach the base station. For instance, in Figure 2A, when $H = 50$ m, D^L values are observed as 1.23, 2.24, 3.31, 4.49, and 5.95 seconds for $d_{net} = 2$, 4, 6, 8, and 10 km, respectively. Increasing the depth of the water also increases D^L values. In Figure 2B, when $d_{net} = 10$ km, D^L values are calculated as 6.02, 6.21, 7.59, 8.04, and 8.50 seconds for $H = 50$, 200, 500, 750, and 1000 m, respectively. Finally, D^L increases as $|W|$ increases since the number of hops to reach the base station gets larger if more nodes are included in the network for a fixed d_{net} and H. When $d_{net} = 10$ km and $H = 50$ m, D^L values are obtained as 5.95, 6.02, and 6.22 seconds for $|W| = 20$, 30, and 40, respectively.

Upper bounds on end-to-end delays when network lifetimes gets maximum values (D^U – in seconds) are shown as a function of d_{net} with the five H values for $|W| = 20$ in Figure 3A, for $|W| = 30$ in Figure 3B, and for $|W| = 40$ in Figure 3C,

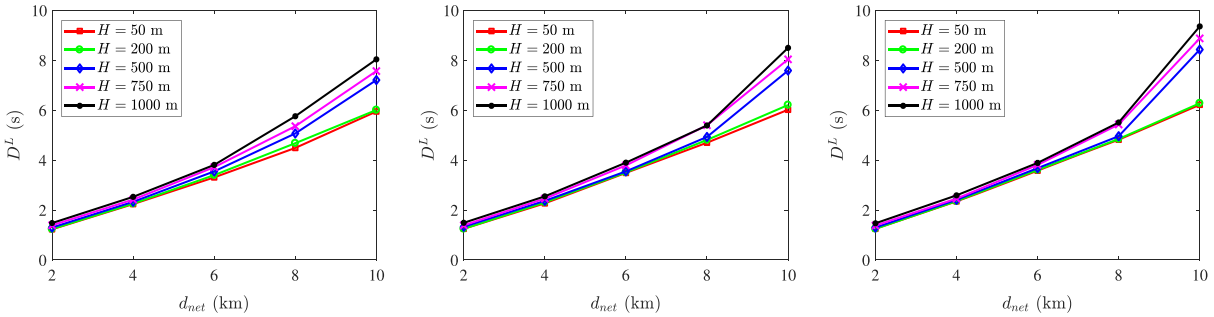

FIGURE 2 Minimum end-to-end delays of the network (D^L) with respect to (wrt.) d_{net}, H, and $|W|$

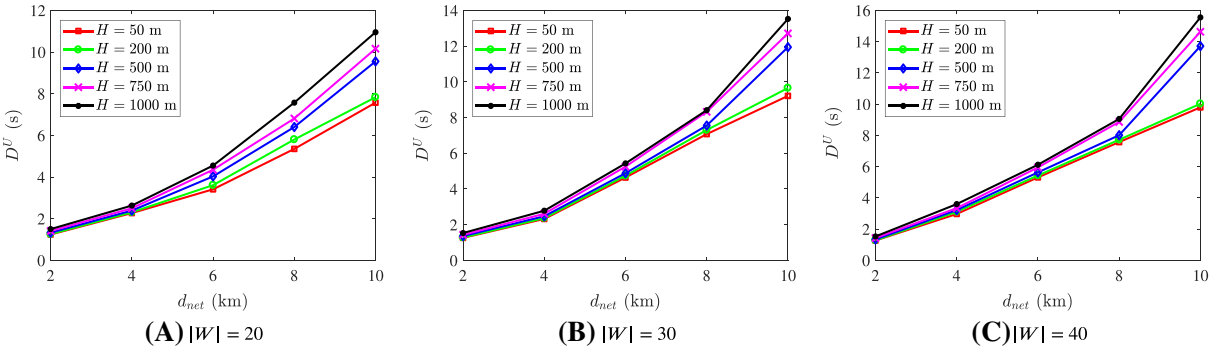

FIGURE 3 Upper bounds on end-to-end delays when network lifetimes are maximum (D^U) wrt. d_{net}, H, and $|W|$

respectively. In this configuration, D^U values are in the interval 1.24 to 15.55 seconds. D^U values also increase as $|W|$, H, or d_{net} increases. For example, in Figure 3A, D^U values are calculated as 1.24, 2.27, 3.41, 5.35, and 7.57 seconds when $H =$ 50 m for $d_{net} = 2$, 4, 6, 8, and 10 km, respectively. When d_{net} is set to 10 km in Figure 3B, D^U values are obtained as 9.21, 9.65, 11.94, 12.71, and 13.52 seconds for $H = 50$, 200, 500, 750, and 1000 m, respectively. Finally, when $d_{net} = 10$ km and $H = 50$ m, D^U values are obtained as 7.57, 9.21 and 9.79 seconds for $|W| = 20$, 30, and 40, respectively.

In Figure 4, we present network lifetimes for the minimum end-to-end delay routing (ie, N_R^L – in rounds) as a function of d_{net} with the five H values for $|W| = 20$ in Figure 4A, for $|W| = 30$ in Figure 4B, and for $|W| = 40$ in Figure 4C, respectively. Our results show that N_R^L values can be as high as 520 924 rounds (in Figure 4Afor $d_{net} = 2$ km and $H = 50$ m) and can be as low as 8426 rounds (in Figure 4Cfor $d_{net} = 10$ km and $H = 1000$ m). In each subfigure, we note that network lifetimes decrease as d_{net} or H increases since the energy required for transmission over longer distances drastically increases. For example, in Figure 4B when $H = 500$ m, N_R^L values are obtained as 493 601 rounds, 257 413 rounds, 88 918 rounds, 42 095 rounds, and 27 251 rounds for $d_{net} = 2$, 4, 6, 8, and 10 km, respectively. In the same figure, when d_{net} is set to 10 km, N_R^L values decrease from 34 299 rounds to 19 629 rounds as H increases from 50 to 1000 m. Moreover, as $|W|$ increases, the amount of traffic flowing in the network increases; hence, critical nodes close to the base station deplete their batteries quickly that result in short network lifetimes. For instance, when $d_{net} = 10$ km and $H = 1000$ m, network lifetimes are observed as 36 862 rounds, 19 629 rounds, and 8426 rounds for $|W| = 20$, 30, and 40, respectively.

In Figure 5, maximum network lifetimes obtained when there are no constraints on the end-to-end delay (ie, N_R^U – in rounds) are provided as a function of d_{net} with the five H values for $|W| = 20$ in Figure 5A, for $|W| = 30$ in Figure 5B, and for $|W| = 40$ in Figure 5C, respectively. N_R^U values are in the interval between 31 130 rounds (in Figure 5C for $d_{net} = 10$ km and $H = 1000$ m) and 556 671 rounds (in Figure 5A for $d_{net} = 2$ km and $H = 50$ m). Similar to the N_R^L case, maximum network lifetimes decrease as d_{net}, H, or $|W|$ increases. For instance, in Figure 5B when $H = 500$ m, N_R^U decreases from 552 767 rounds to 73 154 rounds as d_{net} increases from 2 to 10 km. In the same figure, when d_{net} is set to 10 km, N_R^U values decrease from 83 446 rounds to 56 574 rounds as H increases from 50 to 1000 m. When $d_{net} = 10$ km and $H = 1000$ m, maximum network lifetimes are 87 598 rounds, 56 574 rounds, and 31 130 rounds for $|W| = 20$, 30, and 40, respectively.

As shown in Figures 2 to 5, maximum network lifetimes (ie, N_R^U) cannot be obtained if the minimum end-to-end delay routing is employed. Our results show that the minimum end-to-end delay routing strategy results in 6.42% to 72.93%

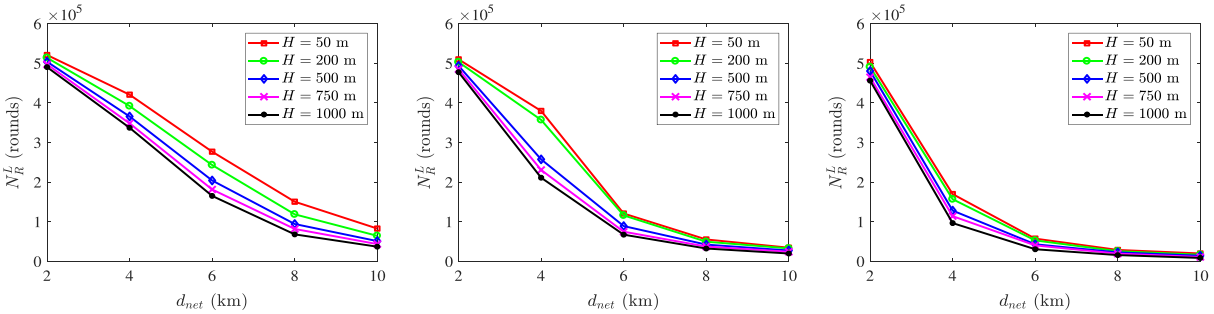

FIGURE 4 Network lifetimes for the minimum end-to-end–delay routing (N_R^L) wrt. d_{net}, H, and $|W|$

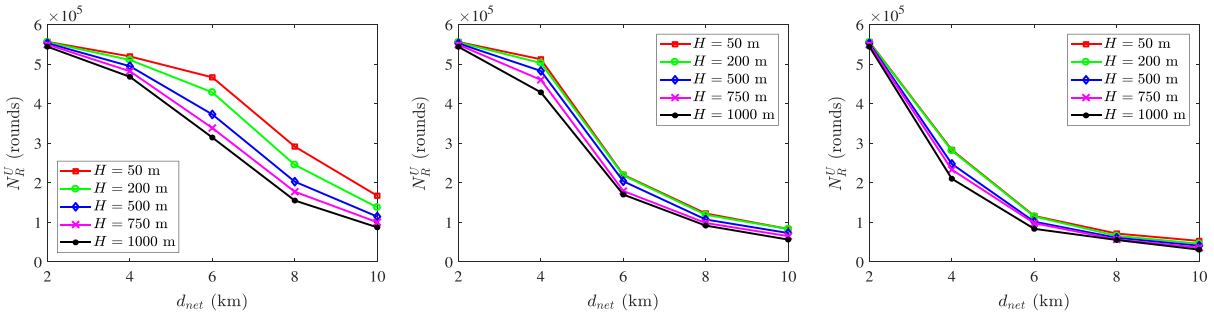

FIGURE 5 Maximum network lifetimes when there are no constraints on the end-to-end delay (N_R^U) wrt. d_{net}, H, and $|W|$

TABLE 1 Minimum end-to-end delays (D^L – in seconds), network lifetimes for the minimum end-to-end delay routing (N_R^L – in rounds), and maximum network lifetimes obtained without any constraints on the end-to-end delay (N_R^U – in rounds) as a function of d_{net} and $|W|$ for $H = 50$, 500, and 1000 m, respectively

		$\|W\| = 20$			$\|W\| = 30$			$\|W\| = 40$		
H (m)	d_{net} (km)	D^L	N_R^L	N_R^U	D^L	N_R^L	N_R^U	D^L	N_R^L	N_R^U
50	2	1.23	520 924	556 671	1.25	509 925	556 371	1.25	503 075	556 401
	4	2.24	420 715	519 796	2.27	379 708	512 490	2.35	169 753	283 395
	6	3.31	276 759	466 861	3.49	120 612	220 375	3.58	57 225	116 298
	8	4.49	150 445	291 792	4.70	55 102	122 598	4.82	28 687	71 835
	10	5.95	82 645	167 484	6.02	34 299	83 446	6.22	19 759	53220
500	2	1.30	503 888	553 128	1.33	493 601	552 767	1.30	480 408	552 674
	4	2.33	365 679	495 061	2.37	257 413	483 128	2.41	128 032	247 984
	6	3.55	204 041	373 102	3.55	88 918	204 025	3.68	42 937	101 839
	8	5.07	94 110	203 033	4.93	42 095	107 368	4.96	22 506	61159
	10	7.21	50 980	114 776	7.59	27 251	73 154	8.43	13 907	41 133
1000	2	1.48	490 335	544 391	1.49	477 645	544 088	1.47	456 153	544 367
	4	2.53	337 143	468 234	2.55	211 050	428 946	2.59	96 464	210 434
	6	3.81	165 065	314 676	3.90	67 179	170 374	3.99	30 407	83 764
	8	5.76	67 959	155 333	5.39	32 239	91 948	5.51	15 644	55 619
	10	8.04	36 862	87 598	8.50	19 629	56 574	9.36	8426	31 130

lower network lifetimes than the maximum network lifetimes obtained when there are no restrictions on the end-to-end delay. In other words, N_R^L values are 6.42% to 72.93% lower than N_R^U values. However, if the minimum end-to-end delay of the network is relaxed by 1.14% to 66.13% (ie, D^L values are increased by 1.14% to 66.13%), then maximum network lifetimes are achieved.

In Table 1, we summarize Figures 2 to 5 such that we present minimum end-to-end delays (D^L – s), network lifetimes for the minimum end-to-end delay routing (N_R^L – in rounds), and maximum network lifetimes obtained without any constraints on end-to-end delay (N_R^U – in rounds) as a function of d_{net} and $|W|$ for $H = 50$, 500, and 1000 m. As seen from this table, the minimum end-to-end delay routing cannot yield maximized network lifetimes. In other words, N_R^L values are lesser than N_R^U values regardless of the network configuration. For example, when $H = 1000$ m, $d_{net} = 10$ km, and $|W| = 20$, we observe the minimum end-to-end delay as 8.04 seconds. If the minimum end-to-end delay routing strategy is employed (ie, the average end-to-end delay of the network is limited to 8.04 seconds), the network lifetime is observed as 36 862 rounds. However, the maximum network lifetime is calculated as 87 598 rounds if there are no restrictions on the end-to-end delay.

In Figure 6, we present network lifetimes (N_R – in axis) and corresponding average end-to-end delays (D – in x axis) as a function of relaxation of the minimum end-to-end delay constraint (in y axis). The results presented in this figure are obtained by gradually solving the optimization problem given in (29) with varying ϵ from D^L to D^U. y axis of each subfigure is denoted by $\tilde{\epsilon}$ such that $\tilde{\epsilon}$ is varied between 0 and 1 (ie, varying ϵ between D^L and D^U). In each subfigure, $|W|$ and H values are fixed while d_{net} values are varied between 2 and 10 km. For the sake of visuality, we choose H values as 50, 500, and 1000 m, respectively.

Our analysis shows that network lifetimes are the lowest when the minimum end-to-end delay routing strategy (ie, $\tilde{\epsilon} = 0$) is employed. As $\tilde{\epsilon}$ (the relaxation of the minimum end-to-end delay) increases, network lifetimes are prolonged. Maximum network lifetimes (N_R^U) are observed when $\tilde{\epsilon} = 1$. For example, when $H = 50$ m, $d_{net} = 10$ km, and $|W| = 20$ (in Figure 6A), network lifetimes are obtained as 82 645 rounds, 165 509 rounds, and 167 484 rounds for $\tilde{\epsilon} = 0$, 0.5, and 1, respectively. In this network configuration, average end-to-end delays are obtained as 5.95, 6.76, and 7.57 seconds for $\tilde{\epsilon} = 0$, 0.5, and 1, respectively. Furthermore, for a fixed $\tilde{\epsilon}$, network lifetimes increase as d_{net} or H decreases. On the other hand, network lifetimes decrease when $|W|$ is increased. Nevertheless, the minimum end-to-end delay routing strategy yields at most 72.93% lower lifetimes than the case when there are no restrictions on the end-to-end delay. Our results also show that drop in N_R^U values becomes negligible when $\tilde{\epsilon} \geq 0.7$. However, in this case, minimum end-to-end delays should be increased by 30.91% to obtain N_R^U values. In general, relaxing the minimum end-to-end delay at most by 66.13% yields N_R^U values. Eventually, average end-to-end delays increase as d_{net}, $|W|$, or H increases, respectively.

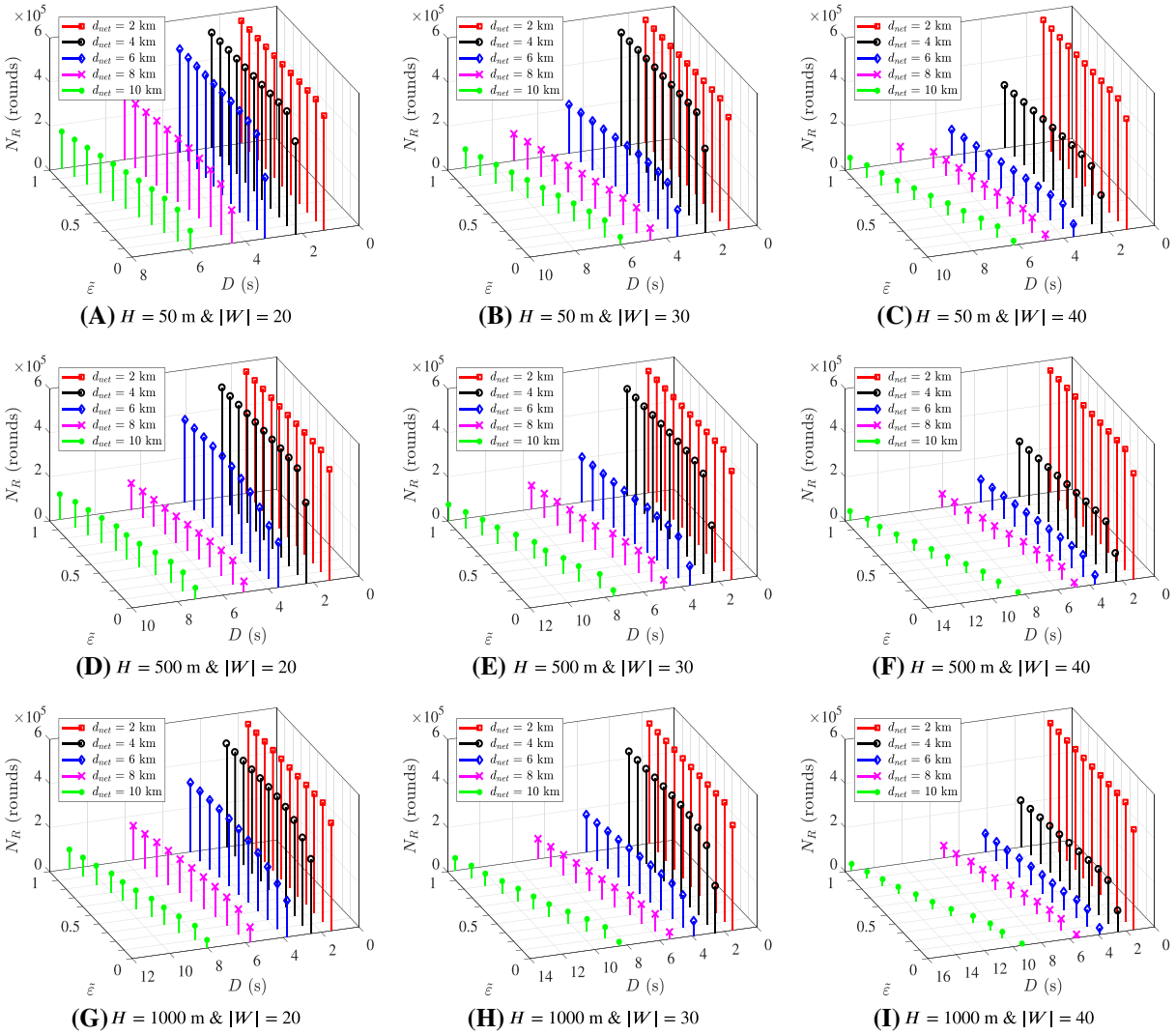

(A) $H = 50$ m & $|W| = 20$ **(B)** $H = 50$ m & $|W| = 30$ **(C)** $H = 50$ m & $|W| = 40$

(D) $H = 500$ m & $|W| = 20$ **(E)** $H = 500$ m & $|W| = 30$ **(F)** $H = 500$ m & $|W| = 40$

(G) $H = 1000$ m & $|W| = 20$ **(H)** $H = 1000$ m & $|W| = 30$ **(I)** $H = 1000$ m & $|W| = 40$

FIGURE 6 Network lifetimes (N_R – in z-axis) and average end-to-end delays (D – in x-axis) as a function of relaxation of the minimum end-to-end delay constraint ($\tilde{\varepsilon}$ – in y-axis) wrt. d_{net}, H, and $|W|$

5 | CONCLUSION

In this manuscript, we investigate the trade-off between the maximum network lifetime and the minimum end-to-end delay in UASNs. We develop a novel MOO framework that maximizes the network lifetime while minimizing the average end-to-end delay of the network. The MOO model incorporates the basic physical layer principles of underwater communications. A detailed link-layer energy dissipation model is employed that uses the power consumption characteristics of WHOI Micromodems. The MOO model is solved by using *ε-constraint method* where the network lifetime is maximized while the minimization of end-to-end delay is defined as a constraint. Our conclusions are itemized as follows:

1. The minimum end-to-end delay routing does not provide maximized network lifetimes which are obtained without any constraints on the end-to-end delay (ie, N_R^U). Our analysis shows that maximum network lifetimes are underestimated at least by 6.42%, at most by 72.93% if the minimum end-to-end delay routing is employed.
2. Maximum possible network lifetimes can exactly be obtained by relaxing the minimum end-to-end delay constraint (ie, increasing D^L) at least by 1.14%, at most by 66.13%.
3. If the minimum end-to-end delay constraint is relaxed at least by 30.91%, then the underestimation of the maximum network lifetime becomes negligible (at most by 1.75%).

ORCID

Huseyin Ugur Yildiz https://orcid.org/0000-0002-1556-2634

REFERENCES

1. Akyildiz IF, Pompili D, Melodia T. Underwater acoustic sensor networks: research challenges. *Ad Hoc Netw*. 2005;3(3):257-279.
2. Ponnavaikko P, Yassin K, Wilson SK, Stojanovic M, Holliday J. Energy optimization with delay constraints in underwater acoustic networks. In: Proc. IEEE Global Communications Conf. (GLOBECOM); 2013; Atlanta, GA, USA:551-556.
3. Felemban M, Felemban E. Energy-delay tradeoffs for underwater acoustic sensor networks. In: Proc. Int. Black Sea Conf. on Communications and Networking (BlackSeaCom); 2013; Batumi, Georgia:45-49.
4. Alhumyani H, Ammar R, Alharbi A, Tolba S. Efficient surface-level gateway deployment using underwater sensing and processing networks. In: Proc. MTS/IEEE OCEANS - Washington; 2015; Washington, DC, USA:1-6.
5. Alhumyani H, Ammar R, Elfouly R, Alharbi A. Heurstic approaches for underwater sensing and processing deployment. In: Proc. Int. Computer Engineering Conf. (ICENCO); 2015; Cairo, Egypt:86-91.
6. Kartha JJ, Jacob L. Delay and lifetime performance of underwater wireless sensor networks with mobile element based data collection. *Int J Distrib Sens N*. 2015;11(5):128757:1-22.
7. Yang H, Liu B, Ren F, Wen H, Lin C. Optimization of energy efficient transmission in underwater sensor networks. In: Proc. IEEE Global Telecommunications Conf. (GLOBECOM); 2009; Honolulu, HI, USA:1-6.
8. Khizar M, Wahid A, Pervaiz K, et al. Enhanced energy efficient depth based routing protocol for underwater WSNs. In: Proc. Int. Conf. on Innovative Mobile and Internet Services in Ubiquitous Computing (IMIS); 2016; Fukuoka, Japan:70-77.
9. Souza FA, Chang BS, Brante G, Souza RD, Pellenz ME, Rosas F. Optimizing the number of hops and retransmissions for energy efficient multi-hop underwater acoustic communications. *IEEE Sens J*. 2016;16(10):3927-3938.
10. Zorzi M, Casari P, Baldo N, Harris AF. Energy-efficient routing schemes for underwater acoustic networks. *IEEE J Sel Area Comm*. 2008;26(9):1754-1766.
11. Yildiz HU, Temiz M, Tavli B. Impact of limiting hop count on the lifetime of wireless sensor networks. *IEEE Commun Lett*. 2015;19(4):569-572.
12. Freitag L, Grund M, Singh S, Partan J, Koski P, Ball K. The WHOI micro-modem: an acoustic communications and navigation system for multiple platforms. In: Proc. MTS/IEEE OCEANS, Vol. 2; 2005; Washington, DC, USA:1086-1092.
13. Ibrahim S, Cui J, Ammar R. Efficient surface gateway deployment for underwater sensor networks. In: Proc. IEEE Symp. on Computers and Communications; 2008; Marrakech, Morocco:1177-1182.
14. Guo Z, Wang B, Cui J. Generic prediction assisted single-copy routing in underwater delay tolerant sensor networks. *Ad Hoc Netw*. 2013;11(3):1136-1149.
15. Ibrahim S, Al-Bzoor M, Liu J, Ammar R, Rajasekaran S, Cui J. General optimization framework for surface gateway deployment problem in underwater sensor networks. *EURASIP J Wirel Comm*. 2013;2013(1):128:1-13.
16. Luo Y, Pu L, Peng Z, Zhou Z, Cui J, Zhang Z. Effective relay selection for underwater cooperative acoustic networks. In: Proc. IEEE Int. Conf. on Mobile Ad-Hoc and Sensor Systems; 2013; Hangzhou, China:104-112.
17. Zheng H, Wu J. Data collection and event detection in the deep sea with delay minimization. In: Proc. IEEE Int. Conf. on Sensing, Communication, and Networking (SECON); 2015; Seattle, WA, USA:354-362.
18. Alhumyani H, Ammar R, Albarakati H, Alharbi A. Deployment strategies for underwater sensing and processing networks. In: Proc. IEEE Symp. on Computers and Communication (ISCC); 2016; Messina, Italy:358-363.
19. Kartha JJ, Jacob L. Network lifetime-aware data collection in underwater sensor networks for delay-tolerant applications. *Sādhanā*. 2017;42(10):1645-1664.
20. Ponnavaikko P, Wilson SK, Stojanovic M, Holliday J, Yassin K. Delay-constrained energy optimization in high-latency sensor networks. *IEEE Sens J*. 2017;17(13):4287-4298.
21. Ibrahim S, Ammar R, Cui J. Surface gateway placement strategy for maximizing underwater sensor network lifetime. In: Proc. IEEE Symp. on Computers and Communications; 2010; Riccione, Italy:342-346.
22. Kartha JJ, Jabbar A, Baburaj A, Jacob L. Maximum lifetime routing in underwater sensor networks using mobile sink for delay-tolerant applications. In: Proc. TENCON - IEEE Region 10 Conf.; 2015; Macao, China:1-6.
23. Cheng C, Li L. Data gathering problem with the data importance consideration in underwater wireless sensor networks. *J Netw Comput Appl*. 2017;78:300-312.
24. Jain S, Fall K, Patra R. Routing in a delay tolerant network. In: Proc. ACM Conf. on Applications, Technologies, Architectures, and Protocols for Computer Communications (SIGCOMM); 2004; Portland, OR, USA:145-158.
25. Pompili D, Melodia T, Akyildiz IF. Routing algorithms for delay-insensitive and delay-sensitive applications in underwater sensor networks. In: Proc. Int. Conf. on Mobile Computing and Networking (Mobicom); 2006; Los Angeles, CA, USA:298-309.
26. Badia L, Mastrogiovanni M, Petrioli C, Stefanakos S, Zorzi M. An optimization framework for joint sensor deployment, link scheduling and routing in underwater sensor networks. In: Proc. ACM Int. Workshop on Underwater Networks (WUWNet); 2006; Los Angeles, CA, USA:56-63.
27. Alsalih W, Hassanein H, Akl S. Delay constrained placement of mobile data collectors in underwater acoustic sensor networks. In: Proc. IEEE Conf. on Local Computer Networks (LCN); 2008; Montreal, Que, Canada:91-97.
28. Ibrahim S, Cui J, Ammar R. Surface-level gateway deployment for underwater sensor networks. In: Proc. IEEE Military Communications Conf. (MILCOM); 2007; Orlando, FL, USA, USA:1-7.
29. Souza FA, Souza RD, Brante G, Pellenz ME, Rosas F. Code Rate, Frequency and SNR optimization for energy efficient underwater acoustic communications. In: Proc. IEEE Int. Conf. on Communications (ICC); 2015; London, UK:6351-6356.

30. Souza F, Souza R, Brante G, Pellenz M, Rosas F, Chang B. Code rate optimization for energy efficient delay constrained underwater acoustic communications. In: Proc. OCEANS - Genova; 2015; Genoa, Italy:1-4.
31. Wang W, Yang L, Zhang Q, Jiang T. Securing on-body IoT devices by exploiting creeping wave propagation. *IEEE J Sel Area Comm*. 2018;36(4):696-703.
32. Wang W, Liu Y, Luo Z, Jiang T, Zhang Q, Nallanathan A. Toward cross-layer design for non-orthogonal multiple access: a quality-of-experience perspective. *IEEE Wirel Commun*. 2018;25(2):118-124.
33. Khan JU, Cho H. A Data gathering protocol using AUV in underwater sensor networks. In: Proc. OCEANS - TAIPEI; 2014; Taipei, Taiwan:1-6.
34. Rodoplu V, Park MK. An Energy-efficient MAC protocol for underwater wireless acoustic networks. In: Proc. MTS/IEEE OCEANS, Vol. 2; 2005; Washington, DC, USA:1198-1203.
35. Urick RJ. *Principles of Underwater Sound*. 3rd ed. Baileys Harbor, WI, USA: Peninsula Pub; 1996.
36. Yildiz HU, Gungor VC, Tavli B. Packet size optimization for lifetime maximization in underwater acoustic sensor networks. *IEEE T Ind Inform*. 2018;15(2):719-729.
37. Mavrotas G. Effective implementation of the *arepsilon*-constraint method in multi-objective mathematical programming problems. *Appl Math Comput*. 2009;213(2):455-465.

How to cite this article: Yildiz HU. Investigation of maximum lifetime and minimum delay trade-off in underwater sensor networks. *Int J Commun Syst*. 2019;32:e3924. https://doi.org/10.1002/dac.3924